



Short communication

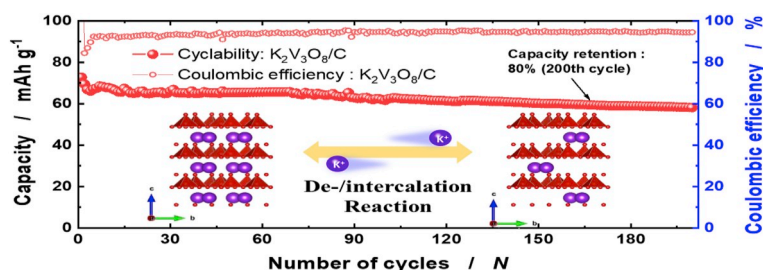
## Potassium vanadate as a new cathode material for potassium-ion batteries

Jae Hyeon Jo<sup>a,1</sup>, Jang-Yeon Hwang<sup>b,1</sup>, Ji Ung Choi<sup>a</sup>, Hee Jae Kim<sup>a</sup>, Yang-Kook Sun<sup>b,\*\*</sup>,  
Seung-Taek Myung<sup>a,\*</sup><sup>a</sup> Department of Nano Technology and Advanced Materials Engineering & Sejong Battery Institute, Sejong University, Gunja-dong, Gwangjin-gu, Seoul, 05006, South Korea<sup>b</sup> Department of Energy Engineering, Hanyang University, Haengdangdong, Seongdong-gu, Seoul, 04763, South Korea

## HIGHLIGHTS

- Crystal structure of  $K_2V_3O_8$  is verified as a new cathode material for potassium storage.
- The  $K_2V_3O_8$  modified with carbon exhibits a reversible capacity of  $75 \text{ mAh g}^{-1}$ .
- The  $K_2V_3O_8$  – carbon composite retains approximately 80% of capacity for 200 cycles.
- Electrochemical reaction is progressed via a reversible  $V^{5+/4+}$  redox pair.
- Potassium ions are extracted and inserted into and out of the crystal structure of  $K_2V_3O_8$ .

## GRAPHICAL ABSTRACT



## ARTICLE INFO

## Keywords:

Potassium vanadate  
Cathode  
Potassium  
Batteries

## ABSTRACT

A new cathode material,  $K_2V_3O_8$ , is reported as a new active material for potassium storage. The  $K_2V_3O_8$  is stabilized into tetragonal structure with  $P4bm$  space group, and we verify the unique crystal structure that is coordinated with four hendecahedra of  $KO_{11}$ ,  $VO_5$ , and  $VO_4$ , in which one  $VO_5$  shares its four oxygens with four  $VO_4$  tetrahedra to produce four penta-shaped voids that allows insertion and extraction of potassium ions. The  $K_2V_3O_8$  modified with carbon exhibits a reversible capacity of  $75 \text{ mAh (g-oxide)}^{-1}$ , and its electrochemical activity originates from the reversible de-/intercalation of potassium ions into/out of the hendecahedrally coordinated  $K_2V_3O_8$ -carbon composite cathode, accompanied by a reversible  $V^{5+/4+}$  redox pair, which is retained for 200 cycles with 80% retention of its initial capacity.

## 1. Introduction

Various potassium insertion materials have been introduced and evaluated for their electrochemical performance as cathodes in potassium-ion batteries (KIBs) [1–4]. K-deficient P2- and P3-type  $K_xMO_2$

( $x \leq 0.7$ , M = transition metal) layered oxides have been extensively investigated as analogues of sodium-ion batteries (SIBs) [5–12]. They exhibit good electrode performances in terms of specific capacities, although they suffer from detrimental phase transitions resulting from the insertion (and extraction) of the large  $K^+$  ions ( $1.38 \text{ \AA}$ ) into (and out

\* Corresponding author.

\*\* Corresponding author.

E-mail addresses: [yksun@hanyang.ac.kr](mailto:yksun@hanyang.ac.kr) (Y.-K. Sun), [smyung@sejong.ac.kr](mailto:smyung@sejong.ac.kr) (S.-T. Myung).<sup>1</sup> These authors contributed equally to this work.

<https://doi.org/10.1016/j.jpowsour.2019.05.064>

Received 25 February 2019; Received in revised form 18 April 2019; Accepted 17 May 2019

Available online 23 May 2019

0378-7753/© 2019 Elsevier B.V. All rights reserved.

of) the crystal structure, which, in turn, limit their cycling stability. Vanadium vanadates including oxides have been extensively investigated as cathode materials for rechargeable batteries activated by monovalent and divalent charge carriers (Li, Na, K and Zn ions) because of their diverse structures and outstanding electrochemical activities resulting from the multiple valence states of vanadium [13–16]. Recently, Lu et al. introduced  $K_2V_3O_8$  as an anode material for KIBs [17], presumably activated by conversion process.

This unique  $K_2V_3O_8$  structure, arranged with alternating K–O layers and V–O layers along the *c*-axis, inspires us to adopt it as a cathode material for KIBs. It is thought that de-/intercalation of potassium ions into/out of this crystal structure is possible because hendecahedrally coordinated  $K^+$ -ion layers are located between the edge-sharing  $VO_5$  and  $VO_4$  assemblies along the *c*-axis. In this study, we firstly introduce the physical and electrochemical properties of  $K_2V_3O_8$ . Due to its poor electrical conductivity, the active material,  $K_2V_3O_8$ , is modified by electro-conducting carbon ( $K_2V_3O_8/C$ ) (Fig. 1a). As per designated, this treatment increases the resulting electrical conductivity to  $10^{-4} S cm^{-1}$  at 25 °C, which enables the present  $K_2V_3O_8$  active for  $K^+$  extraction and insertion for 200 cycles, delivering a reversible capacity of 75 mAh (g-oxide) $^{-1}$ . In this paper, we report on physical and electrochemical characteristics of  $K_2V_3O_8$  as a potassium storage material.

## 2. Experimental

$K_2V_3O_8$  was synthesized through a typical solvothermal synthesis method; in detail, KOH and  $V_2O_5$  (in a 4:3.6 stoichiometric ratio) were dissolved in anhydrous ethanol (80 mL), and then the solution was uniformly mixed. The mixture solution was transferred into the autoclave, which was then heated at 200 °C for two days and subsequently cooled to room temperature. The resultant powders were washed with ethanol and deionized water several times, and then the resultant was

dried 80 °C for one day. To fabricate the  $K_2V_3O_8/C$  composite, the as-prepared  $K_2V_3O_8$  powders were blended with 5 wt % of carbon black (Denka Black) by high energy ball milling (As One, PM-001, Japan) at 350 r.p.m. for 12 h. The synthesis details are illustrated in Fig. 1a.

The structural properties of the  $K_2V_3O_8/C$  composite were analyzed via Raman spectroscopy (Renishaw, United Kingdom). *Ex situ* X-ray absorption near-edge structure (XANES) analysis was performed to monitor the variation of the oxidation state of vanadium. The XANES measurements were performed at the 6D Crystallography and Scattering UNIST-PAL (XAFS) beamline at Pohang Accelerator Laboratory (PAL) in Pohang, South Korea. The V K-edge XANES data were obtained in total-electron-yield mode.

The cathode was prepared by blending the active material ( $K_2V_3O_8$  and  $K_2V_3O_8/C$ ), Super P carbon black (C), and polyvinylidene fluoride (PVdF) binder (80:10:10 in weight) with *N*-methyl-2-pyrrolidone (NMP) to form a slurry. For the composite electrode, the composition varied to 84.2:5.8:10, since the ratio of active material and carbon was 95:5 in weight. This gives the same formulation of electrodes in considered of the added carbons and active materials. The slurry was applied on Al foil using a doctor blade and then dried at 110 °C under. The prepared electrode was assembled in R2032 coin cells with potassium metal as an anode and 0.5 M KPF<sub>6</sub> in ethylene carbonate (EC) – dimethyl carbonate (DEC) (1:1 by volume) solvent as an electrolyte in an Ar-filled glove box. The cells were tested in the operating range between 1.0 and 4.2 V (20 mA g $^{-1}$ ) at 25 °C. To identify the  $K^+$  ion diffusion coefficient, the galvanostatic intermittent titration technique (GITT) measurement of the electrode were conducted at each 10-min step of charge (depot-assiation)/discharge (potassiation) followed by a 30-min relaxation step in half cell. The full cells were fabricated by paring the proposed  $K_2V_3O_8/C$  composite as the cathode and hard carbon as the anode. The full cell balance is achieved by controlling the capacity ratio of the anode to the cathode (N/P ratio) to be 1.2 : 1. Prior to full cell

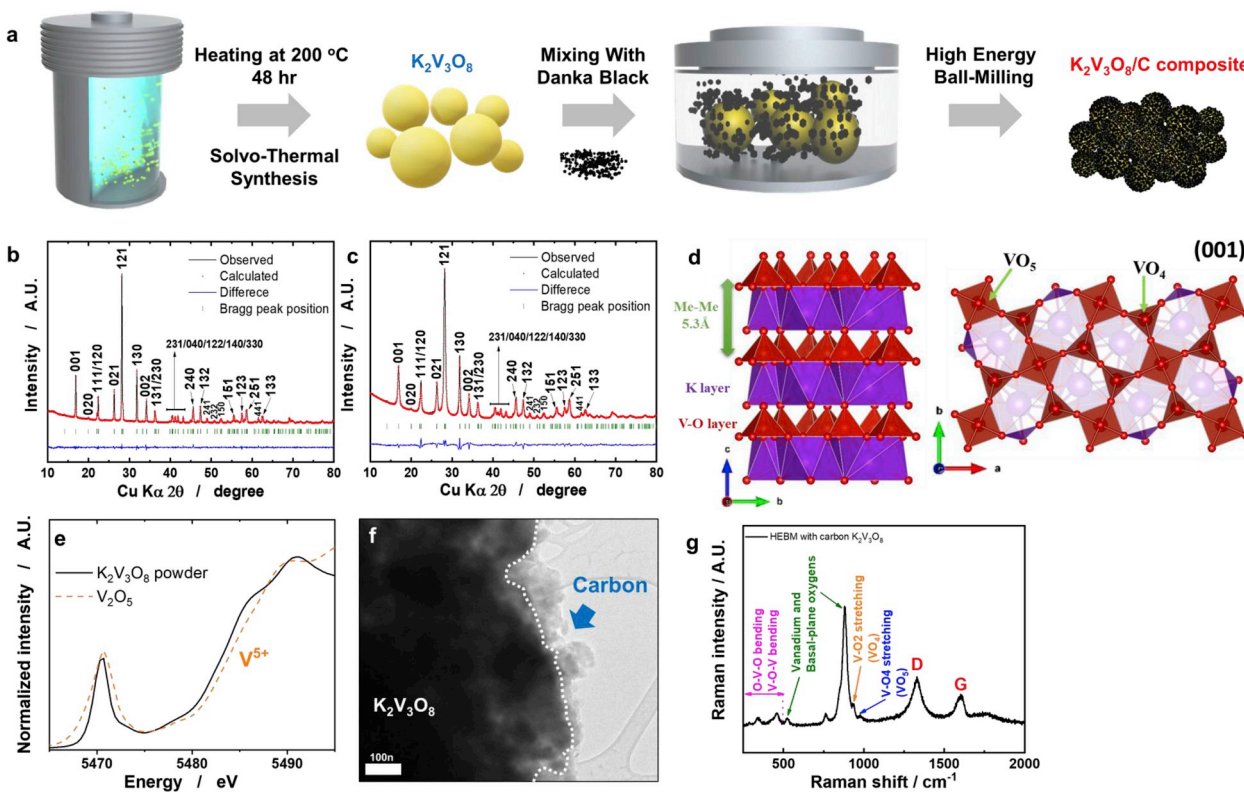


**Fig. 1.** (a) Schematic of the synthesis and ball-milling method to prepare the  $K_2V_3O_8/C$  composite; results of Rietveld refinement of XRD data for (b)  $K_2V_3O_8$  and (c)  $K_2V_3O_8/C$  composite; (d) crystal structure of  $K_2V_3O_8$  determined using the refinement results; (e) V K-edge XANES spectra obtained from  $K_2V_3O_8$  powders; (f) bright-field TEM image of  $K_2V_3O_8/C$  composite; (g) Raman spectrum of the  $K_2V_3O_8/C$  composite.

fabrication, both cathode and anode were pre-cycled to remove the irreversible capacity loss in the first cycle [18]. The full cell was tested in the voltage range from 0.5 to 3.8 V at a current of 20 mA g<sup>-1</sup>.

### 3. Results and discussion

Results of the Rietveld refinement of the XRD data for the as-synthesized K<sub>2</sub>V<sub>3</sub>O<sub>8</sub> and the composite blended with carbon black are shown in Fig. 1b and c. The structural refinement was carried out assuming a tetragonal structure with *P4bm* space group (ICDD: 98-000-1925). The observed XRD patterns agreed with the calculated one for both the as-synthesized (Fig. 1b) and the composite (Fig. 1c) despite the broadening of the XRD peaks after the compositization. The crystal structure of K<sub>2</sub>V<sub>3</sub>O<sub>8</sub> is sketched in Fig. 1d that was determined using the structural information obtained from the Rietveld refinement for both K<sub>2</sub>V<sub>3</sub>O<sub>8</sub> and the blended composite (Table S1 and Table S2). Seen from the (001) projection (Fig. 1d), there are two vanadium 5+ atoms for each vanadium 4+ atom, giving an average oxidation state of vanadium of 4.67+ (Fig. 1e), with the V<sup>5+</sup> atoms occupying different crystallographic sites than the V<sup>4+</sup> atoms. Specifically, the vanadium and oxygen form VO<sub>5</sub> and VO<sub>4</sub>, in which one VO<sub>5</sub> shares its four oxygens with four VO<sub>4</sub> tetrahedra to produce four penta-shaped voids, below which four hendecahedra of KO<sub>11</sub> are present perpendicular to the *a-b* plane. Each

hendecahedron shares faces to align the potassium along the *a-b* plane. These two layers repeat along the *c*-axis with an interlayer distance of 5.3 Å, providing a large channel for K<sup>+</sup>-ion transport along the *a-b* plane. As shown in the SEM image in Figs. S1a and b, K<sub>2</sub>V<sub>3</sub>O<sub>8</sub> is composed with submicron-sized particles (0.5–1 μm). The broadening of the XRD pattern of the composite is associated with reduction in the particle size of the K<sub>2</sub>V<sub>3</sub>O<sub>8</sub> after the high-energy blending process (Figs. S1c and d). The elemental mapping data obtained using energy-dispersive X-ray spectroscopy (EDX) for the selected area in the SEM image show the presence of K, V, O, and C in the blended composite (Fig. S1e). The bright-field TEM image of the blended product shows the presence of carbon on the K<sub>2</sub>V<sub>3</sub>O<sub>8</sub> particles after the mechanical blending (Fig. 1f). Thermogravimetric analysis of the composite in air indicated a weight loss of approximately 5 wt % between 400 and 700 °C, which corresponds to the removal of the carbon that was present in the blended composite (Fig. S1f). The Raman spectrum provides further information on the K<sub>2</sub>V<sub>3</sub>O<sub>8</sub>/C composite material (Fig. 1g): (1) V–O–V and O–V–O bending vibrations (205–500 cm<sup>-1</sup>), (2) vanadium and basal-plane oxygen (530 and 880 cm<sup>-1</sup>), (3) V–O<sub>x</sub> stretching (940 cm<sup>-1</sup> and 980 cm<sup>-1</sup>), and (4) D band (1350 cm<sup>-1</sup>) and G (1600 cm<sup>-1</sup>) band peaks for the carbonaceous material [19].

The electrochemical behavior of K<sub>2</sub>V<sub>3</sub>O<sub>8</sub> and K<sub>2</sub>V<sub>3</sub>O<sub>8</sub>/C electrodes was tested in nonaqueous K cells in the voltage range between 1.0 and

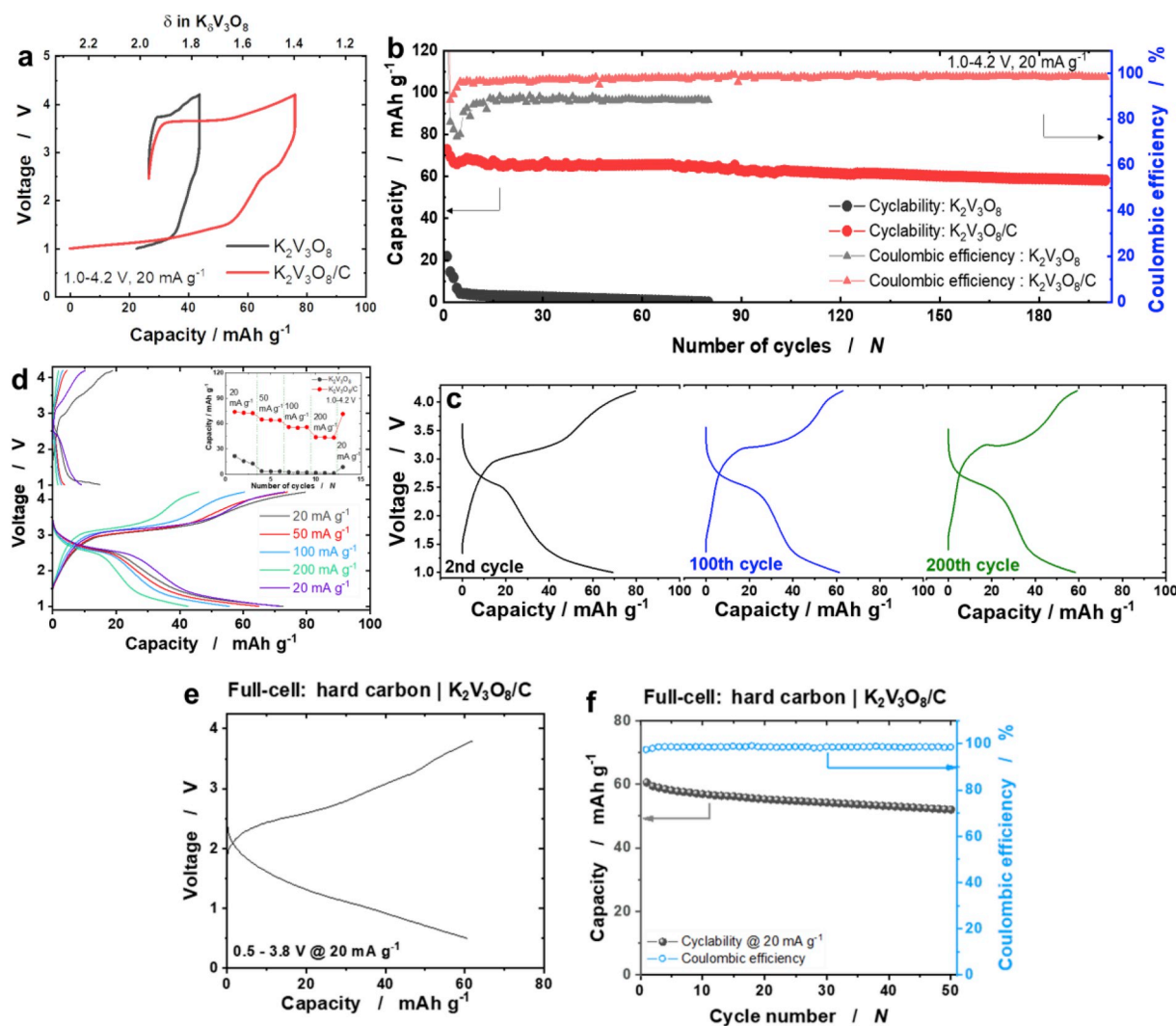


Fig. 2. (a) The initial charge and discharge profile of K<sub>2</sub>V<sub>3</sub>O<sub>8</sub> and K<sub>2</sub>V<sub>3</sub>O<sub>8</sub>/C composite electrodes; (b) cyclability and (c) selected charge-discharge curves of K<sub>2</sub>V<sub>3</sub>O<sub>8</sub>/C composite electrodes; (d) rate capability of K<sub>2</sub>V<sub>3</sub>O<sub>8</sub> and K<sub>2</sub>V<sub>3</sub>O<sub>8</sub>/C composite electrodes in which the inset presents cyclability at different rates; (e) initial charge-discharge curve; (f) cycling performance of hard carbon |K<sub>2</sub>V<sub>3</sub>O<sub>8</sub>/C full cell in the voltage range of 0.5–3.8 V at 20 mA g<sup>-1</sup>.

4.2 V at 20 mA g<sup>-1</sup>. Fig. 2a shows the resulting charge-discharge curves for the K<sub>2</sub>V<sub>3</sub>O<sub>8</sub> and K<sub>2</sub>V<sub>3</sub>O<sub>8</sub>/C cathodes. The theoretical capacity of K<sub>2</sub>V<sub>3</sub>O<sub>8</sub> is calculated to be 149.2 mAh (g-oxide)<sup>-1</sup>. The as-synthesized K<sub>2</sub>V<sub>3</sub>O<sub>8</sub> delivered small charge and discharge capacities of 20 and 22 mAh (g-oxide)<sup>-1</sup>, respectively (Fig. 2a), indicating that K<sub>2</sub>V<sub>3</sub>O<sub>8</sub> cannot properly accommodate K<sup>+</sup> ions in its structure because of its poor electrical conductivity [20]. In contrast, the K<sub>2</sub>V<sub>3</sub>O<sub>8</sub>/C electrode was able to deliver a charge capacity of approximately 49 mAh (g-oxide)<sup>-1</sup>, which is close to the theoretical value assuming the oxidation of vanadium from 4.67 to +5+. On charging (oxidation), a voltage plateau was observed at 3.65 V, after which the voltage increased to 4.2 V. On discharging (reduction), the K<sub>2</sub>V<sub>3</sub>O<sub>8</sub>/C exhibited a large polarization, and the corresponding slope and voltage plateau appeared at low voltages as a downslope in the range of 3.2–2.7 V and a voltage plateau at 2.5 V. Extending the voltage cut-off limit to 1 V is effective in delivery of more capacity. Thus, the total capacity obtained on discharge was 75 mAh (g-oxide)<sup>-1</sup>. Considering the valence state when fully charged, approximately 5+, it is reasonable that the oxidized V<sup>5+</sup> is reduced to close to V<sup>4.5+</sup> based on the theoretical capacity, leading to K<sub>2.32</sub>V<sub>3</sub>O<sub>8</sub>/C. The cycle performance of the K<sub>2</sub>V<sub>3</sub>O<sub>8</sub>/C electrode showed good reversibility for 200 cycles, with approximately 80% of capacity retention (Fig. 2b and c). The rate capability of the K<sub>2</sub>V<sub>3</sub>O<sub>8</sub>/C electrode was also acceptable even at 200 mA g<sup>-1</sup>, still delivering 60% versus the capacity obtained at 20 mA g<sup>-1</sup>, whereas the K<sub>2</sub>V<sub>3</sub>O<sub>8</sub> cathode showed no capacity at the same current (Fig. 2d). This improvement in the capacity, retention, and rate capability is attributable to the surface modification of the K<sub>2</sub>V<sub>3</sub>O<sub>8</sub> by the electrically conductive carbon. Higher polarization observed only at the first cycle when tested at 20 mA g<sup>-1</sup> (Fig. 2d), compared to the data tested at 50 mA g<sup>-1</sup>. As observed from the second charge-discharge curve for cycling test in Fig. 2c and rate test shown with purple color in Fig. 2d, the operation voltage was stabilized during extensive cycles (Fig. 2c), and the resulting polarization at 20 mA g<sup>-1</sup> is lower than that seen at 50 mA g<sup>-1</sup> (Fig. 2d). Such behavior may be related to the establishment of diffusion path or low Coulombic efficiency at the first cycle, which is usually observed in Na or K-deficient transition metal compounds such as Na<sub>2/3</sub>MnO<sub>2</sub> [21] and K<sub>0.5</sub>MnO<sub>2</sub> [10]. As shown in Fig. 1a, the electrical conductivity of K<sub>2</sub>V<sub>3</sub>O<sub>8</sub> was

significantly improved from 5.4 × 10<sup>-7</sup> S cm<sup>-1</sup> (K<sub>2</sub>V<sub>3</sub>O<sub>8</sub>) to 6.7 × 10<sup>-4</sup> S cm<sup>-1</sup> by the addition of the conducting carbon. Furthermore, we measured diffusivity of K<sup>+</sup> ions for K<sub>2</sub>V<sub>3</sub>O<sub>8</sub> and K<sub>2</sub>V<sub>3</sub>O<sub>8</sub>/C using GITT techniques. The GITT measurement of the electrode were conducted at each 10-min step of charge (depotassiation)/discharge (potassiation) followed by a 30-min relaxation step. The diffusion coefficient (D<sub>K<sup>+</sup></sub>) was calculated from Eq. (1) derived by Huggins [22,23].

$$D_{K^+} = \frac{4}{\pi} \left( \frac{V_m}{FA} \right)^2 \frac{I^0 \left( \frac{d\epsilon}{d\delta} \right)^2}{\left( \frac{d\epsilon}{dt^{1/2}} \right)^2} \text{ for } t \ll \frac{\left( \frac{d}{2\pi} \right)^2}{D_{K^+}} \quad (1)$$

where V<sub>m</sub> is the molar volume, F is the Faraday constant, A is the contact area between the electrolyte and sample, I<sup>0</sup> is the applied constant electric current, dε/dδ is the slope of the coulometric titration curve, and dε/dt is the slope of the short-time transient voltage change. The equation is valid for times shorter than the diffusion, (d/2π)<sup>2</sup>/D<sub>K<sup>+</sup></sub>, where d is the average diameter of the grains (~1 μm on average). The D<sub>K<sup>+</sup></sub> values derived from Eq. (1) are based on the following assumption: V<sub>m</sub> remains unchanged with the variation in potassium content in the compounds. During charge-discharge process, the measured diffusion coefficient of K<sup>+</sup> ions in K<sub>2</sub>V<sub>3</sub>O<sub>8</sub>/C ranged from 10<sup>-9</sup>–10<sup>-14</sup> cm<sup>2</sup> s<sup>-1</sup>, however, the K<sub>2</sub>V<sub>3</sub>O<sub>8</sub> exhibited lower diffusion coefficient of 10<sup>-10</sup>–10<sup>-15</sup> cm<sup>2</sup> s<sup>-1</sup>, as shown in Fig. S2. This implies that the K<sub>2</sub>V<sub>3</sub>O<sub>8</sub> modified by electro-conducting carbon facilitates the diffusion of K<sup>+</sup> ions into and out of the K<sub>2</sub>V<sub>3</sub>O<sub>8</sub>.

To demonstrate the efficacy of the K<sub>2</sub>V<sub>3</sub>O<sub>8</sub>/C composite, full cells were fabricated by pairing the proposed K<sub>2</sub>V<sub>3</sub>O<sub>8</sub>/C composite as the cathode and hard carbon as the anode. The full cell was tested in the voltage range of 0.5–3.8 V at a current of 20 mA g<sup>-1</sup>. As shown in Fig. 2e and f, the hard carbon |K<sub>2</sub>V<sub>3</sub>O<sub>8</sub>/C full-cell delivered a high reversible capacity of 61 mAh (g-oxide)<sup>-1</sup> and was retained 87% of its initial capacity for 50 cycles.

From the charge-discharge curves in Fig. 2a, we assumed that the vanadium in K<sub>2</sub>V<sub>3</sub>O<sub>8</sub>/C was oxidized and reduced during charge-discharge process. To confirm the variation in the oxidation state,

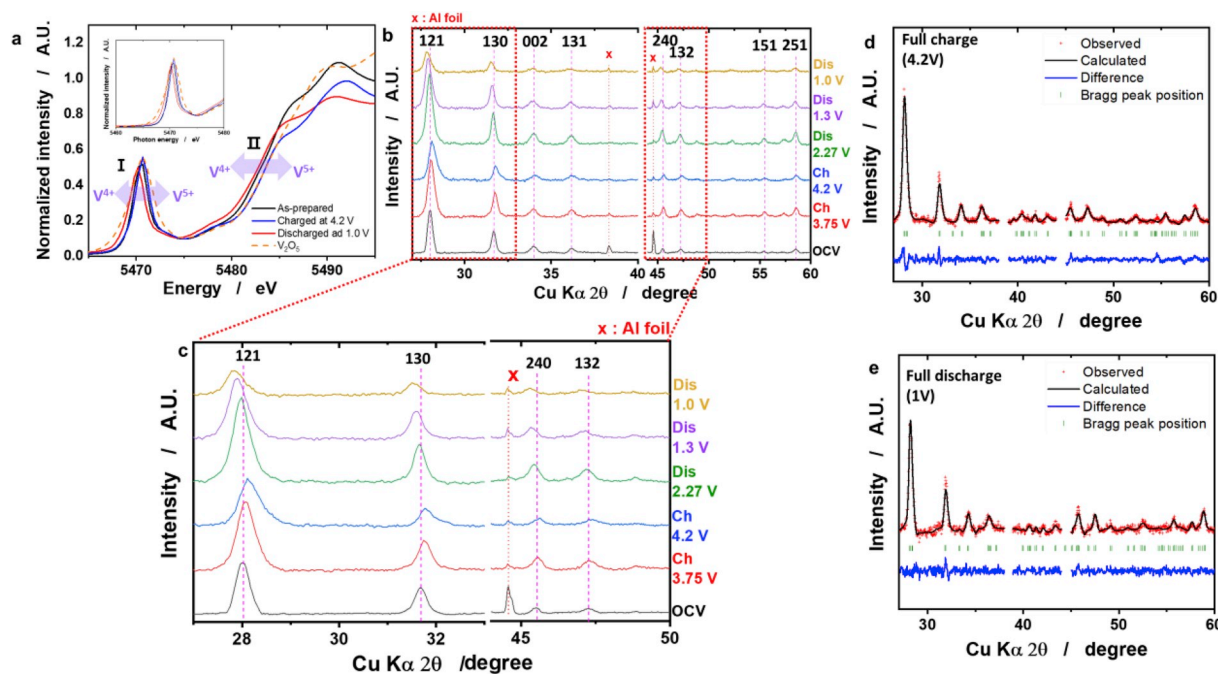


Fig. 3. (a) *Ex situ* V K-edge XANES spectra obtained from charged and discharged K<sub>2</sub>V<sub>3</sub>O<sub>8</sub>/C composite electrodes; (b) *ex situ* XRD patterns of K<sub>2</sub>V<sub>3</sub>O<sub>8</sub>/C composite measured during charge and discharge and (c) the corresponding magnified XRD patterns; Rietveld refinement results of (d) fully charged and (e) discharged K<sub>2</sub>V<sub>3</sub>O<sub>8</sub>/C composite electrodes.

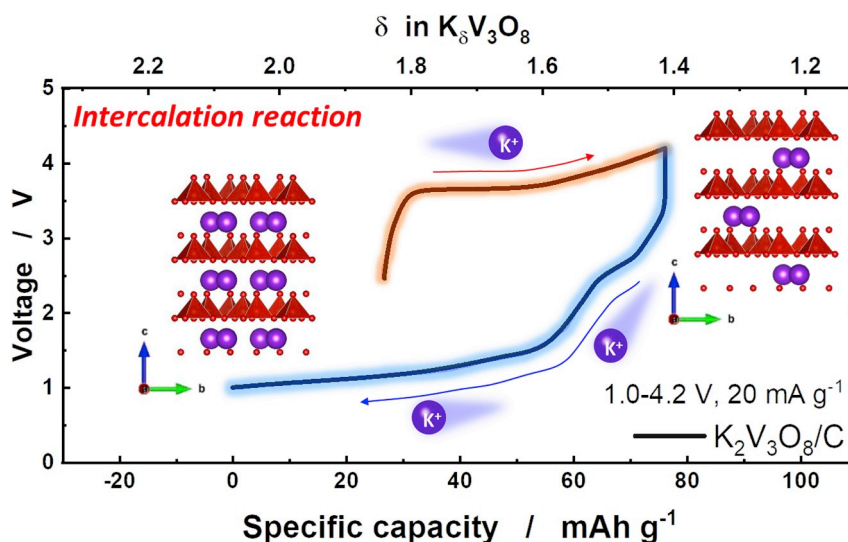


Fig. 4. Summary of the electrochemical reaction process for  $\text{K}_2\text{V}_3\text{O}_8/\text{C}$  composite electrode.

vanadium K-edge XANES spectra were obtained for the as-synthesized composite, its charged (4.2 V), and discharged (1.0 V) states (Fig. 3a). For the fresh  $\text{K}_2\text{V}_3\text{O}_8/\text{C}$  electrode, the oxidation state of V is lower than that of  $\text{V}^{5+}_2\text{O}_5$ . Charging the  $\text{K}_2\text{V}_3\text{O}_8/\text{C}$  electrode to 4.2 V resulted in a slight shift of the K-edge spectrum toward higher photon energy. This shift represents an increase in the average oxidation state of vanadium toward 5+. The XRD patterns also show slight changes (Fig. 3b); namely, shifts of the XRD peaks toward higher angle, as can be clearly observed in the magnified XRD pattern (Fig. 3c). Compared to those of the fresh state, the calculated lattice parameters decreased for the charged electrode (Fig. 3d, Tables S3 and S4). Based on the shift of the K-edge XANES spectra and decrease in the lattice parameters, it is suggested that the oxidation reaction occurred through the extraction of  $\text{K}^+$  ions from the crystal structure. After discharge to 1.0 V, the pre-edge peak and edge resonance positions of the fully discharged electrode shifted lower energy value than that of the as-prepared state, indicating that the content of intercalated  $\text{K}^+$  (discharge) is larger than those of the fresh material and depotassiated state (charged) from the  $\text{K}_2\text{V}_3\text{O}_8/\text{C}$  structure as shown in Fig. 2a. This affects the shift of XRD peaks toward lower angle as a result of reduction of vanadium on discharge, accompanied by  $\text{K}^+$  insertion into the structure [24]. And these were reflected in the XRD pattern (Fig. 3b and c). The calculated lattice parameters were slightly larger than those of the fresh  $\text{K}_2\text{V}_3\text{O}_8/\text{C}$  (Fig. 3e, Tables S3 and S5). These variations are mainly ascribed to the electrochemical reduction of the vanadium. There are two vanadium atoms with  $\text{V}^{4+}$  (denoted as V1 as  $\text{V}^{4+}\text{O}_5$ ) and  $\text{V}^{5+}$  (referred as V2 as  $\text{V}^{5+}\text{O}_4$ ) in crystallographic sites of  $\text{K}_2\text{V}_3\text{O}_8$ , giving an average oxidation state of vanadium of 4.67+ (Fig. 1e). From this consideration,  $\text{V}1^{4+}$  from  $\text{VO}_5$  is oxidized to  $\text{V}1^{5+}$  on charge as evidenced from XANES (Fig. 3a). Rietveld refinement of XRD data of  $\text{K}_2\text{V}_3\text{O}_8/\text{C}$  charged to 4.2 V indicated reduction of bonding distance between  $\text{V}1\text{--O}$  in  $\text{VO}_5$  (Fig. 3d and Tables S4 and S6). Interestingly, the bonding distance between  $\text{V}1\text{--O}$  in  $\text{VO}_5$  increased relative to that of  $\text{V}2\text{--O}$  in  $\text{VO}_4$  after discharging to 1 V (Fig. 3e and Tables S5 and S6). This suggests that the  $\text{V}1^{4+}$  from  $\text{VO}_5$  participates in the electrochemical reaction more actively; hence, most of capacity is delivered by the redox of the  $\text{V}1^{4+/5+}$  redox pair during electrochemical reaction that is consistent with the discharge capacity in consideration of the average oxidation state of V as  $\text{V}^{4.5+}$  on discharge, which is consistent with oxidation state verified by XANES (Fig. 3a). Therefore, it is possible that the  $\text{VO}_4$  plays an important role to support the framework of the crystal structure, while the main redox reaction is contributed by redox pair of  $\text{V}^{4+/5+}$  from  $\text{VO}_5$  in  $\text{K}_2\text{V}_3\text{O}_8$ . From these results, we confirmed that the discharge reaction progresses through insertion of  $\text{K}^+$

into hendecehedrally coordinated potassium sites. The charge-discharge reaction process is summarized in Fig. 4. Notably, the crystal structure was stable even after extensive cycling (Fig. S3), showing its great potential for potassium ion storage. We compared electrochemical performances of the present  $\text{K}_2\text{V}_3\text{O}_8/\text{C}$  with reported vanadium-based cathode materials for KIBs [1,2,13,25]. As shown in Table S7, the  $\text{K}_2\text{V}_3\text{O}_8/\text{C}$  material presents comparable electrode performances to the reported materials in terms of capacity and cyclability as a cathode material for KIBs.

#### 4. Conclusion

In summary, we introduce  $\text{K}_2\text{V}_3\text{O}_8$  with hendecehedrally coordinated potassium ions as a cathode material for KIBs. The large  $\text{K}^+$  ions are inserted and extracted into and out of the crystal structure of carbon-modified  $\text{K}_2\text{V}_3\text{O}_8$  accompanying a  $\text{V}^{5+/4+}$  redox pair. The  $\text{K}_2\text{V}_3\text{O}_8/\text{C}$  cathode delivers a reversible capacity of  $75 \text{ mAh g}^{-1}$ , and the capacity is retained for 200 cycles in K cells. We believe that the findings presented herein will contribute to the development of efficient cathode materials for KIBs.

#### Acknowledgments

This research was supported by the National Research Foundation of Korea (NRF), funded by the Ministry of Education, Science and Technology of Korea (MEST) (NRF-2015M3D1A1069713) and supported by the research fund of Hanyang University (HY-2019).

#### Appendix A. Supplementary data

Supplementary data to this article can be found online at <https://doi.org/10.1016/j.jpowsour.2019.05.064>.

#### References

- [1] K. Chihara, A. Katogi, K. Kubota, S. Komaba, *Chem. Commun.* 53 (2017) 5208–5211.
- [2] W.B. Park, S.C. Han, C. Park, S.U. Hong, U. Han, S.P. Singh, Y.W. Jung, D. Ahn, K.-S. Sohn, M. Pyo, *Adv. Energy Mater.* 8 (2017) 1703099.
- [3] A. Eftekhari, Z. Jian, X. Ji, *ACS Appl. Mater. Interfaces* 9 (2017) 4404–4419.
- [4] J.-Y. Hwang, S.-T. Myung, Y.-K. Sun, *Adv. Funct. Mater.* 28 (2018) 1802938.
- [5] K. Sada, B. Senthilkumar, P. Barpanda, *Chem. Commun.* 53 (2017) 8588–8591.
- [6] N. Naveen, W.B. Park, S.C. Han, S.P. Singh, Y.H. Jung, D. Ahn, K.-S. Sohn, M. Pyo, *Chem. Mater.* 30 (2018) 2049–2057.
- [7] J.Y. Hwang, J.S. Kim, T.-Y. Yu, S.-T. Myung, Y.K. Sun, *Energy Environ. Sci.* 11 (2018) 2821–2827.

- [8] H. Kim, J.C. Kim, S.-H. Bo, T. Shi, D.-H. Kwon, G. Ceder, *Adv. Energy Mater.* 7 (2017) 1700098.
- [9] C. Vaalma, G.A. Giffin, D. Buchholz, S. Passerini, *J. Electrochem. Soc.* 163 (2016) A1295–A1299.
- [10] H. Kim, D.-H. Seo, J.C. Kim, S.-H. Bo, L. Liu, T. Shi, G. Ceder, *Adv. Mater.* 29 (2017) 1702480.
- [11] C. Liu, S. Luo, H. Huang, Z. Wang, A. Hao, Y. Zhai, Z. Wang, *Electrochem. Commun.* 92 (2017) 150–154.
- [12] X. Wang, X. Xu, C. Niu, J. Meng, M. Huang, X. Liu, Z. Liu, L. Mai, *Nano Lett.* 17 (2017) 544–550.
- [13] L. Deng, X. Niu, G. Ma, Z. Yang, L. Zeng, Y. Zhu, L. Guo, *Adv. Funct. Mater.* 28 (2018) 1800670.
- [14] X. Xiong, Z. Wang, X. Li, H. Guo, *Mater. Lett.* 76 (2012) 8–10.
- [15] H. He, G. Jin, H. Wang, X. Huang, Z. Chen, D. Sun, Y. Tang, *J. Mater. Chem.* 2 (2014) 3563–3570.
- [16] C. Xia, J. Guo, Y. Lei, H. Liang, C. Zhao, H.N. Alshareef, *Adv. Mater.* 30 (2017) 1705580.
- [17] M. Lu, K. Wang, H. Ke, Q. Hu, Z. Liu, H. Wu, *Mater. Lett.* 232 (2018) 224–227.
- [18] J.H. Jo, J.U. Choi, A. Konarov, H. Yashiro, S. Yuan, L. Shi, Y.-K. Sun, S.-T. Myung, *Adv. Funct. Mater.* 8 (2018) 1705968.
- [19] K.-Y. Choi, P. Lemmens, V.P. Gnezdilov, B.C. Sales, M.D. Lumsden, *Phys. Rev. B* 85 (2012) 144434.
- [20] S.R. Robert, J.S. Samuel, in: *Solid State Chemistry: Proceedings*, vol. 13, National Bureau of Standards, Washington, D.C., 1972.
- [21] J. Zheng, P. Yan, W.H. Kan, C. Wang, A. Manthiram, *J. Electrochem. Soc.* 3 (2016) A584.
- [22] W. Weppner, R.A. Huggins, *J. Electrochem. Soc.* 124 (1977) 1569.
- [23] D.W. Dees, S. Kawauchi, D.P. Abraham, J. Prakash, *J. Power Sources* 189 (2009) 263.
- [24] D. Yuan, X. Hu, J. Qian, F. Pei, F. Wu, R. Mao, X. Ai, H. Yang, Y. Cao, *Electrochim. Acta* 116 (2014) 300.
- [25] J. Han, G.-N. Li, F. Liu, M. Wang, Y. Zhang, L. Hu, C. Dai, M. Xu, *Chem. Commun.* 53 (2017) 1805.